# Laser Doppler Anemometry Study of a Turbulent Jet in Crossflow

Oktay Özcan*
*Yıldız Technical University, 34349 Istanbul, Turkey*
and
Poul Scheel Larsen†
*Technical University of Denmark, DK-2800 Lyngby, Denmark*

## Introduction

A JET in crossflow is an important practical problem encountered in turbine cooling, fuel injection, thrust vectoring (vertical/short takeoff and landing aircraft), and missile control. Experiments by Fric and Roshko[1] and Kelso et al.[2] show that there exists a complex vortical flow in the near field. The main vortical structures include the horseshoe vortex, the counter-rotating bound vortex pair (CVP), the jet shear-layer vortices, and the upright wake vortices. The majority of experimental data existing in the literature were obtained with conventional hot-wire anemometry, which is insensitive to flow direction and can give large errors in regions of high turbulence. The present Note investigates the effect of velocity ratio on both mean flow topology and skin friction for a round jet exhausting normal to a flat plate raised from the side wall of a wind tunnel. Two-component laser Doppler anemometry (LDA) was employed to measure mean velocity in three mutually perpendicular planes of the flowfield near the jet exit. The choice of test conditions has been guided by a wish to supplement existing numerical and experimental studies, notably those of Yuan et al.[3] and Kim et al.[4]; hence, a jet-to-crossflow velocity ratio of 3.3 was chosen. The lower velocity ratio of 1.3 was included in the study to show parametric effects for a turbulent incoming jet. Thanks to an artificially thickened turbulent boundary layer developing on the flat plate, skin friction could be determined from velocity measurements close to the wall on the plane of symmetry. Results to be presented are based on a database,[5] which includes distributions of three components of mean velocity, vorticity, turbulent kinetic energy, and all Reynolds stresses.

## Experimental Method

The experiments were carried out in a low-speed wind tunnel with test section dimensions of 300 × 600 mm. The jet issued normal to a flat-plate insert that had a length of 1950 mm, a width of 598 mm, and a thickness of 10 mm. The jet axis was located 1350 mm downstream of the leading edge of the plate. The distance between the flat plate and the opposite sidewall was 264 mm. The jet flow, produced by shop air, issued at the downstream end of a 2.5-m-long and straight perspex pipe of inside diameter (i.e., jet diameter) of $D = 24$ mm. The experiments were conducted at a nominal freestream velocity (crossflow velocity) of $U_\infty = 1.50$ m/s. Two different values of jet bulk velocity $W_j$ were employed to produce jet-to-crossflow velocity ratios $R = W_j/U_\infty$ of 1.3 and 3.3, nominally. The crossflow Reynolds number based on jet diameter $D$ and freestream velocity $U_\infty$ was $Re_c = 2.4 \times 10^3$ nominally.

Special consideration was given to establish and document fully developed and self-preserved incoming flows in the pipe and on the flat plate, respectively. The incoming turbulent boundary-layer profile was measured approximately four jet diameters upstream of the jet center, where the thickness of boundary layer and laminar sublayer was 70 and 1 mm, respectively. Hence it was possible to determine surface shear stress from velocity measurements close to the wall in the plane of symmetry. Such results were based on a minimum of three measurement points in the laminar sublayer within one to seven wall units from the wall. The upstream reference value of skin-friction coefficient was $C_f = 0.0043$.

A two-component, four-beam, fiber-optic-based LDA system (DANTEC55X) was used to measure the mean velocity components ($U$, $V$, $W$) defined in a Cartesian coordinate system with origin at the jet exit in the center of pipe. The crossflow and the jet flow are in the $x$ and $z$ directions, respectively. Data were obtained in three mutually perpendicular planes (at different times) by using three different configurations of the LDA optics. Common velocity components of two such planes agreed to within 4%, which is taken as a measure of accuracy of the mean velocity components. The accuracy of the coefficient of skin friction is estimated to be ±0.0004. A Laskin-type seeding generator utilizing shop air and a glycerol/water mixture was used to generate seed particles that had a mean diameter of 2 to 4 $\mu$m. Separate seeding generators were used in seeding the crossflow and the jet flow.

## Results and Discussion

Figure 1 shows a vector map of the mean velocity ($U$, $W$) and corresponding sectional streamlines in the $y = 0$ plane of symmetry near the jet exit for $R = 3.3$. Assuming that the mean velocity normal to the $y = 0$ plane is zero, the sectional streamlines and streamlines are identical. Diamond symbols indicate the jet trajectory that is the mean streamline originating from the center of the jet very close to the flat plate. Letter M indicates the maximal length vector that has a magnitude of $4.1U_\infty$. For the purpose of marking the actual position of the jet, Yuan and Street[6] report that this so-called "streamline trajectory" is superior to jet trajectories based on alternative definitions. Figure 1 shows a deflection of the streamlines toward the plate surface upstream of the jet. This is because of the attachment of the crossflow following the boundary-layer separation that generates the horseshoe vortex. The jet trajectory shown in Fig. 1 is roughly 15% higher than the computed jet trajectory of Yuan et al.[3] This discrepancy is probably caused by differences in the state of the incoming boundary layer, which is laminar in the computations and turbulent in the experiments of the present study. A good matching of jet trajectories is essential for a satisfactory agreement between experimental and computational flowfields.

Critical point theory[7,8] states that sectional streamlines have properties consistent with those of continuous vector fields and can have a restricted number of singular (critical) points, which are called nodes, saddles, and foci. Topology of streamlines on the plane of symmetry is similar for the two velocity ratios considered. A node $N$ downstream of the jet is observed for both cases. The node is located at ($x^* = x/D = 2.0$, $z^* = z/D = 0.2$) and ($x^* = 1.4$, $z^* = 0.15$) for $R = 3.3$ and 1.3, respectively. For $R = 3.3$ there exists a focus F around ($x^* = -0.7$, $z^* = 0.05$), which is the center of the horseshoe

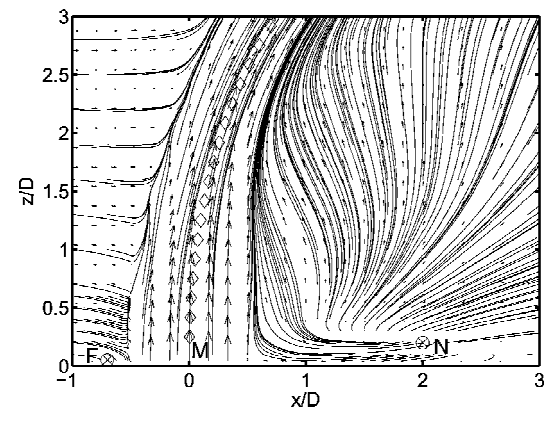


**Fig. 1 Mean velocity ($U$, $W$) vector map and sectional streamlines in the $y = 0$ plane for $R = 3.3$: symbols, jet trajectory; M, maximal length vector; N, node; and F, focal point.**

Received 19 December 2001; revision received 17 March 2003; accepted for publication 21 March 2003. 

*Professor, Faculty of Mechanical Engineering.
†Professor, Department of Mechanical Engineering.

vortex. Hypothesized streamline patterns given by Kelso et al.[2] and Özcan and Larsen[5] involve a saddle and a focus-type singularity along the upstream jet-crossflow interface. However, accurate determination of these singular points is difficult. Three-dimensional color plots presented by Meyer et al.[9] for $R = 3.3$ show that crossflow streamlines close to the flat plate are deflected towards the plane of symmetry and then are lifted steeply away from the plate downstream of the jet. It appears that this tornado-like rise of crossflow fluid within the CVP originates approximately from the same $(x^*, z^*)$ location as that of the singular point N shown in Fig. 1. It can be speculated that the crossflow fluid enters into the plane of symmetry at the singular point N, where it is dispersed in all directions. This hypothesis is supported by flow-visualization studies,[10] which indicate that the jet fluid remains in a cylindrical shear layer and shows up in the plane of symmetry only around the jet trajectory.

Figures 2a and 2b show vector maps of the mean velocity $(U, V)$ and corresponding sectional streamlines in the symmetric half of the $z^* = z/D = 0.17$ plane near the jet exit for $R = 3.3$ and 1.3, respectively. The circular dashed line indicates the edge of the jet pipe. Letter M indicates the maximal length vector that has a magnitude of 1.6 and $1.3U_\infty$ in Figs. 2a and 2b, respectively. In contrast to the streamline topology in the plane of symmetry, the topology of sectional streamlines near the jet exit is rather dissimilar for $R = 3.3$ and 1.3. This indicates that the formation of the CVP is at different stages near the jet exit for the two velocity ratios. For $R = 1.3$ there exists a focus F at $(x^* = 0.55, y^* = 0.23)$ and a saddle S at $(x^* = 0.45, y^* = 0)$. For the larger velocity ratio of $R = 3.3$, on the other hand, there are two foci [F1 at $(x^* = 0.40, y^* = 0.42)$ and F2 at $(x^* = 0.24, y^* = 0.38)$], which indicate that the clockwise rotating leg of the CVP is split into two parts. In this case the singular point on the axis of symmetry is not a saddle but a node N located at $(x^* = 0.31, y^* = 0)$. Additionally, there is a saddle point S at $(x^* = 0.28, y^* = 0.1)$. Topological arguments stipulate that there exists an additional saddle point (not shown) between F1 and F2. The center of each CVP (located around the foci) moves closer to the line of symmetry with decreasing velocity ratio. A large portion of the CVP is out of the field of view in Figs. 2a and 2b. The downstream boundary of the reverse streamwise velocity region is marked by a saddle point of singularity (outside the field of view) located on the line of symmetry at $x^* = 2.3$ and 1.4 for $R = 3.3$ and 1.3, respectively. The larger reverse flow region for the larger velocity ratio indicates a stronger CVP.

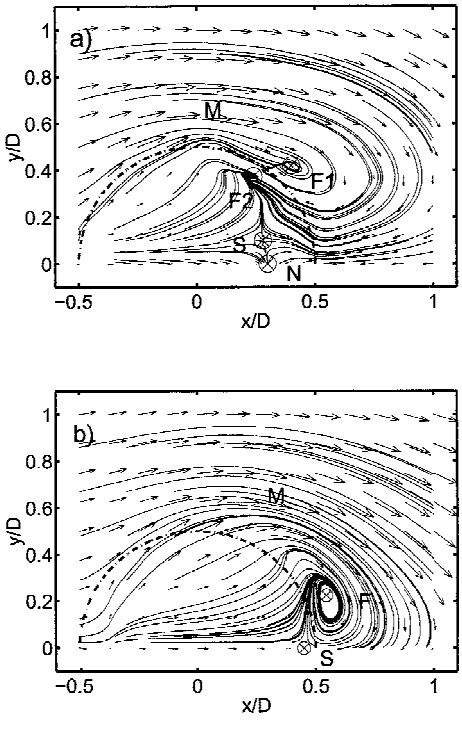


**Fig. 2 Mean velocity $(U, V)$ vector maps and sectional streamlines in the symmetric half of the $z/D = 0.17$ plane for a) $R = 3.3$ and b) $R = 1.3$: – – –, semicircle, jet exit; M, maximal length vector; N, node; S, saddle point; and F, focal point.**

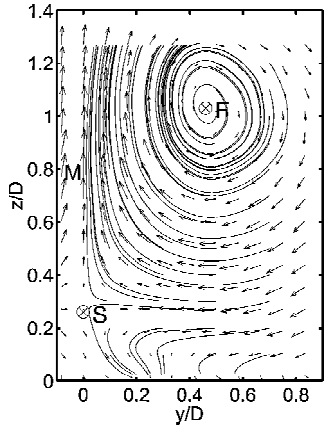


**Fig. 3 Mean velocity $(V, W)$ vector maps and sectional streamlines in the $x/D = 2.4$ plane for $R = 1.3$: M, maximal length vector; S, saddle point; and F, focal point.**

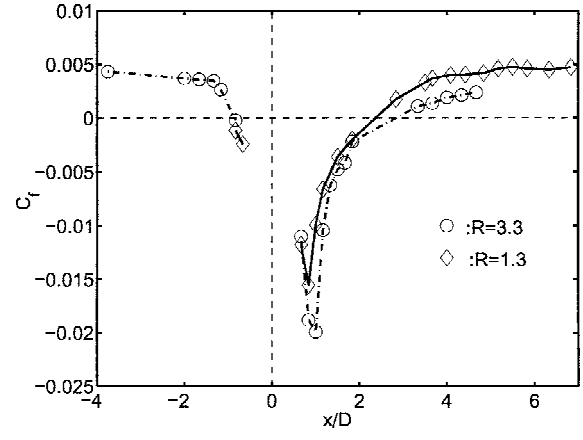


**Fig. 4 Variation of the skin-friction coefficient $C_f$ on the flat-plate center plane along the $x$ axis for $R = 3.3$ and 1.3.**

Figure 3 shows a vector map of the mean velocity $(V, W)$ and the corresponding sectional streamlines in the $x^* = 2.4$ plane for $R = 1.3$. Letter M indicates the maximal length vector that has a magnitude of $0.4U_\infty$. Some deviation from symmetry with respect to the $y = 0$ line can be observed for small values of $z/D$. Focus F indicates the center of the CVP's leg in the $y > 0$ region. A dividing sectional streamline originating from the saddle point S forms the boundary between the counter-rotating CVP and the horseshoe vortex pair. When $R$ increases from 1.3 to 3.3, the saddle and focus points move to $(y^* = 0, z^* = 0.4)$ and $(y^* = 1.5, z^* = 2.6)$, respectively.

Figure 4 gives the variation of the skin-friction coefficient $C_f$ (wall shear stress divided by dynamic pressure of freestream) on the flat plate in the center plane along the $x$ axis for $R = 3.3$ and 1.3. Data were not obtained for $x/D < -1$ for $R = 1.3$, and $C_f$ is not defined for $-0.5 < x/D < 0.5$. In the reverse flow region the absolute values of $C_f$ are up to four times larger than those of the incoming boundary layer. The dip in $C_f$ downstream of the jet exit is larger for $R = 3.3$, which indicates a higher scavenging action of the horseshoe vortex. Downstream values of $C_f$, however, are largest for $R = 1.3$, which is probably caused by the energizing effect of CVP being closer to the surface for this case.

## Conclusions

Mean velocity data obtained by LDA for two velocity ratios reveal the critical points defining the CVP and the horseshoe vortex in a jet in crossflow. Topologies of streamlines in the $y^* = 0$ and $x^* = 2.4$ planes are similar for the velocity ratios of 3.3 and 1.3. In contrast, topologies of sectional streamlines near the jet exit plane $(z^* = 0.17)$ are dissimilar, indicating different strengths and stages of CVP formation.

## Acknowledgments

The first author acknowledges his sabbatical leave from the Technical University of Istanbul and his receipt of a grant in scope of the

NATO Science Fellowship Programme by the Scientific and Technical Research Council of Turkey and also the financial support of the Technical University of Denmark Department of Energy Engineering and Department of Mechanical Engineering. Thanks are also owed to Knud Erik Meyer for his expert assistance in LDA measurements.

## References

[1]Fric, T. F., and Roshko, A., "Vortical Structure in the Wake of a Transverse Jet," *Journal of Fluid Mechanics*, Vol. 279, 1994, pp. 1–47.

[2]Kelso, R. M., Lim, T. T., and Perry, A. E., "An Experimental Study of Round Jets in Cross Flow," *Journal of Fluid Mechanics*, Vol. 306, 1996, pp. 111–144.

[3]Yuan, L. L., Street, R. L., and Ferziger, J. H., "Large-Eddy Simulations of a Round Jet in Crossflow," *Journal of Fluid Mechanics*, Vol. 379, 1999, pp. 71–104.

[4]Kim, K. C., Kim, S. K., and Yoon, S. Y., "PIV Measurements of the Flow and Turbulent Characteristics of a Round Jet in Crossflow," *Journal of Visualization*, Vol. 3, No. 2, 2000, pp. 157–164.

[5]Özcan, O., and Larsen, P. S., "An Experimental Study of a Turbulent Jet in Cross-flow by Using LDA," Dept. of Mechanical Engineering, Technical Univ. of Denmark, Rept. MEK-FM 2001-02, Lyngby, June 2001.

[6]Yuan, L. L., and Street, R. L., "Trajectory and Entrainment of a Round Jet in Crossflow," *Physics of Fluids*, Vol. 10, No. 9, 1998, pp. 2323–2335.

[7]Tobak, M., and Peake, D. J., "Topology of Three-Dimensional Separated Flows," *Annual Review of Fluid Mechanics*, Vol. 14, 1982, pp. 61–85.

[8]Perry, A. E., and Chong, M. S., "A Description of Eddying Motions and Flow Patterns Using Critical-Point Concept," *Annual Review of Fluid Mechanics*, Vol. 19, 1987, pp. 125–155.

[9]Meyer, K. E., Özcan, O., and Westergaard, C. H., "Flow Mapping of a Jet in Cross-flow with Stereoscopic PIV," *Journal of Visualization*, Vol. 5, No. 3, 2002, pp. 225–231.

[10]Lim, T. T., New, T. H., and Luo, S. C., "On the Development of Large-Scale Structures of a Jet Normal to a Cross Flow," *Physics of Fluids*, Vol. 13, No. 3, 2001, pp. 770–775.

R. M. C. So
*Associate Editor*

# Test Data Uncertainty Analysis Algorithm of NASA Ames Wind Tunnels

Norbert M. Ulbrich*
*Sverdrup Technology, Inc.,*
*Moffett Field, California 94035-1000*

## Nomenclature

$B$ = systematic uncertainty
$\boldsymbol{B}$ = systematic uncertainty vector
$B'$ = correlated systematic uncertainty
$b_k$ = systematic uncertainty of an elemental error source
$e_i$ = component of the unit precision uncertainty vector
$\boldsymbol{e}_i$ = unit precision uncertainty vector
$e_k$ = component of the unit systematic uncertainty vector
$\boldsymbol{e}_k$ = unit systematic uncertainty vector
$i$ = index of a measured variable
$j$ = index of a measured variable
$k$ = index of an elemental error source
$M$ = total number of elemental error sources
$N$ = total number of measured variables
$P$ = precision uncertainty
$\boldsymbol{P}$ = precision uncertainty vector
$p_i$ = component of the precision uncertainty vector
$R_i$ = range of a measured variable
$r$ = result
$U$ = total uncertainty
$x_i$ = measured variable
$\Delta x$ = step size used for the numerical differentiation
$\delta_{ij}$ = Kronecker delta
$\varepsilon$ = relative machine precision
$\lambda$ = characteristic scale
$\mu$ = index of a measured variable
$\xi$ = index of an elemental error source

Received 23 February 2002; revision received 16 September 2002; accepted for publication 3 March 2003. 

*Senior Aerodynamicist. Member AIAA.

## Introduction

A TEST data uncertainty analysis system is being developed for NASA Ames wind tunnels. After reviewing some of the available literature on uncertainty analysis,[1–3] it was decided to implement Meyn's[3] uncertainty propagation methodology in the uncertainty analysis system. His methodology is mathematically identical with the traditional methodology that is recommended in the AIAA Standard[1] on wind-tunnel test data uncertainty analysis. Meyn's approach, however, makes complex uncertainty correlations between measurements easier to understand as no covariance matrix is needed.

In the first part of this Technical Note, a new derivation of Meyn's uncertainty propagation law is presented. Then, it is shown how Meyn's vector approach can be extended to precision uncertainty estimates. Issues related to the numerical calculation of partial derivatives are also discussed. Finally, key elements of the proposed uncertainty analysis algorithm are summarized.

## Estimate of Uncertainty

In most practical applications a result is given by a data reduction equation of the type

$$r = r(x_1, \ldots, x_N) \tag{1}$$

where $x_1, \ldots, x_N$ are measured variables. The square of the total uncertainty of the result equals the sum of the squares of the systematic and precision uncertainties. Then, we get[2]

$$U^2(r) = B^2(r) + P^2(r) \tag{2}$$

where $B(r)$ is the systematic uncertainty and $P(r)$ is the precision uncertainty of the result.

### Systematic Uncertainty

In general, using the traditional uncertainty analysis methodology, the systematic uncertainty $B(r)$ of a result is given by the following formula[2]:

$$B(r) = \sqrt{\sum_{i=1}^{N}\left(\frac{\partial r}{\partial x_i}\right)^2 B^2(x_i) + 2\sum_{i=1}^{N-1}\sum_{j=i+1}^{N}\frac{\partial r}{\partial x_i}\frac{\partial r}{\partial x_j}B'(x_i, x_j)} \tag{3a}$$

$$B^2(x_i) = \sum_{k=1}^{M} b_k^2(x_i) \tag{3b}$$

$$B'(x_i, x_j) = \sum_{k=1}^{M} b_k(x_i) b_k(x_j) \tag{3c}$$

where the systematic uncertainty $B(x_i)$ and the correlated systematic uncertainty $B'(x_i, x_j)$ of a measured variable $x_i$ are a function of uncertainties $b_k(x_i)$ of elemental error sources.